Chemical Science

Accepted Manuscript

This article can be cited before page numbers have been issued, to do this please use: A. P. Thomas, L. Palanikumar, M. T. Jeena, K. Kim and J. Ryu, *Chem. Sci.*, 2017, DOI: 10.1039/C7SC03169F.

ROYAL SOCIETY OF CHEMISTRY

rsc.li/chemical-science

View Article Online
DOI: 10.1039/C7SC03169F

Journal Name

ARTICLE

Cancer-mitochondria-targeted photodynamic therapy with supramolecular assembly of HA and a water soluble NIR cyanine dye

Ajesh P. Thomas,[†] L. Palanikumar,[†] M.T. Jeena, Kibeom Kim, and Ja-Hyoung Ryu*

Received 00th January 20xx,
Accepted 00th January 20xx

DOI: 10.1039/x0xx00000x

www.rsc.org/

Mitochondria-targeted cancer therapies have proven to be more effective than other similar non-targeting techniques, especially in photodynamic therapy (PDT). Indocyanine dye derivatives, particularly IR-780 are widely known for their PDT utility. However, poor water solubility, dark toxicity, and photobleaching are limiting factors of these dyes, which otherwise show promise based on their good absorption in the near-infrared (NIR) region and mitochondria targeting ability. Herein, we introduce an indocyanine derivative (IR-Pyr) that is highly water soluble, exhibiting higher mitochondrial targetability and better photostability than IR-780. Further, electrostatic interactions between the positively charged IR-Pyr and negatively charged hyaluronic acid (HA) were utilized to construct a micellar aggregate that is selective toward cancer cells. The cancer mitochondria-targeted strategy assures high PDT efficacy that proved by in vitro and in vivo experiments.

Introduction

In the last decade, photodynamic therapy (PDT) has emerged as a potential therapeutic tool for treating various tumors, and has attained elevated interest based on noninvasive nature of the technique.[1] The technique works via a combination of three components; photosensitizer (PS) or drug, light, and oxygen. Controlled generation and deactivation of short-lived cytotoxic agents within a cell upon irradiation of a prodrug or photosensitizer is the key step in PDT.[2] Light excitation of a dye causes an intermolecular triplet-triplet energy transfer that generates the highly reactive cytotoxic agent, singlet oxygen ($^1O_2$), within a target region, which in turn destroys the affected cells. The technique has precise spatial and temporal control and is externally switchable.[3] However, the efficacy of the technique is limited by issues including (i) poor water solubility of photosensitizers; leads to aggregation in aqueous media (during blood circulation) and altered photophysical, photochemical and biological properties from those otherwise expected: (ii) a low molar extinction coefficient in the far-red region of light, which is critical for deep tissue penetration, (iii) low production of singlet oxygen due to severe hypoxia caused by oxygen consumption and vascular shutdown in tumors, and (iv) non-targetability of the sensitizer that induces dark toxicity.[4] These constraints demand novel molecular designs and delivery strategies to improve the therapeutic efficacy.[5]

Recently, targeting mitochondria; vital organelles for cell survival, as they play a central role in energy production and apoptotic pathways, have been recognized as an efficient strategy in different therapeutic techniques by disturbing the normal function.[6] Particularly in PDT, mitochondria-targeting sensitizers can overcome the hypoxia factor, resulting in high efficacy.[7] Indocyanine dyes, mainly IR780 derivatives are known for their mitochondria-targeting ability and good absorption in the far-red region of light that makes it suitable for PDT applications.[8] However, the inherent fast photobleaching, hydrophobicity, dark toxicity and low dose tolerance of the dye limit it's PDT efficacy, which in turn originates from self-aggregation of the dye in aqueous media.[9] As an alternative, a general strategy employed is encapsulation of the PS or drugs in the hydrophobic core of a polymeric or lipid-based nanocarrier.[10]

Among these, hyaluronic acid (HA), a negatively charged polysaccharide, has been extensively used for cancer selective drug delivery applications, due to overexpressed HA receptors (CD44) in cancer cells.[11] The excellent biocompatibility and unique biological characteristics of the polymer make it suitable for these applications. Herein, we developed a water soluble indocyanine derivative, **IR-Pyr** with preferential accumulation in mitochondria and better photostability than that of IR-780. Further, electrostatic interactions between the positively charged **IR-Pyr** and the negatively charged HA polymer were used to generate micellar aggregates (**HA-IR-Pyr**) that preferentially accumulate in CD44 overexpressing tumor, are cleaved by hyaluronidase inside the cell, and localize in the cancer mitochondria (Fig. 1a) to induce high PDT efficacy during laser irradiation, which has been proven by in vitro and in vivo experiments.

Department of chemistry, School of Natural Sciences
Ulsan National Institute of Science and Technology (UNIST)
Ulsan-44919, South Korea

† These authors contributed equally to this work
Electronic Supplementary Information (ESI) available:
See DOI: 10.1039/x0xx00000x

View Article Online
DOI: 10.1039/C7SC03169F

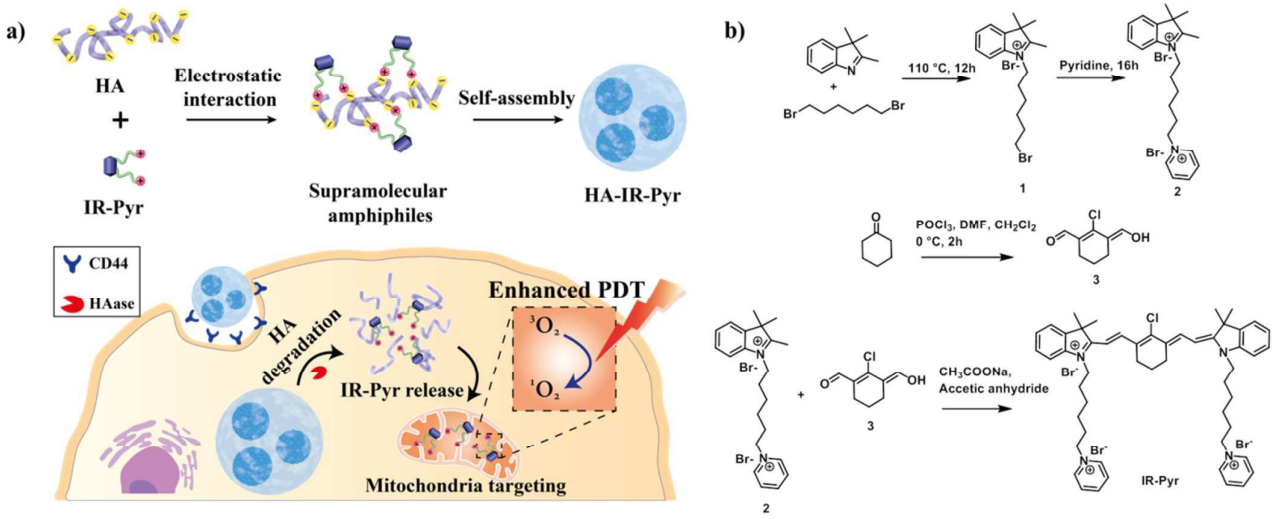

Fig. 1 a) Schematic representation showing the formation of **HA-IR-Pyr**, receptor mediated (CD44) cellular uptake and cancer-mitochondria localization for enhanced PDT, b) Synthetic scheme for **IR-Pyr**.

Results and discussion

Synthesis and photophysical properties of IR-Pyr and HA-IR-Pyr

IR-Pyr was synthesized via a multi-step synthetic strategy (Fig. 1b). In the first step, 2,3,3-trimethylindoline was condensed with 1,6-dibromohexane to get compound **1**. Pyridinium ion substituted trimethylindolinium bromide (**2**) was synthesized by reacting compound **1** in excess pyridine at 110 ^{o}C. In the final step condensation of **2** and **3** in acetic anhydride with sodium acetate gave a crude mixture of IR-Pyr in green color. The mixture was purified by column chromatography in silica gel column, followed by high performance liquid chromatography (HPLC) purification to yield the desired product (**IR-Pyr**). Formation of precursors and **IR-Pyr** were confirmed by using different spectroscopic techniques such as ^{1}H NMR, ^{13}C NMR and ESI-MS (Fig. S1-S12). **IR-Pyr** was highly soluble in water (log P -0.16), which justified the molecular design with pyridinium ion for mitochondrial targeting. The optical behaviour of the molecule in aqueous media was investigated that showed a major absorption peak at 776 nm with a hump at 706 nm (Fig. S13). Interestingly, the photo and dark stability of **IR-Pyr** was found to be significantly better in comparison with IR-780 (Fig. 2a and 2b), which was monitored by measuring changes in the absorption spectra with respect to time. The improved stability of **IR-Pyr** was attributed to increased water solubility, which prevented aggregation in aqueous media.

To improve cancer selectivity, a supramolecular polymer was constructed by utilizing the electrostatic interaction between the positively charged **IR-Pyr** and the negatively charged HA polymer. Formation of micellar aggregates (**HA-IR-Pyr**) was confirmed by DLS, Zeta potential and TEM analyses. The average size of the spherical micellar aggregate was 60 nm (Fig. 2c, S14) in DLS, whereas the TEM analysis showed

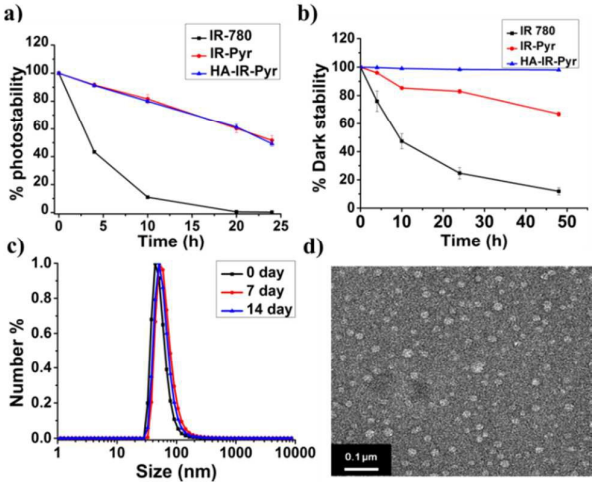

Fig. 2. Comparison of a) photostability, b) dark stability in PBS, c) DLS, d) TEM for **HA-IR-Pyr**.

an average particle size of 30 nm (Fig. 2d). A negative zeta potential was observed (-40 mv), demonstrating the formation of the polymer-coated supramolecular structure (Fig. S15). The encapsulation efficiency of the dye was calculated using absorption spectra and was found to be 0.33. Further, it was found to be stable at 4 ^{o}C for up to 90 days, as determined by DLS analysis (Fig S16).

Photostability of the micellar aggregate was similar to that of **IR-Pyr**, whereas dark stability significantly improved upon HA coating (Fig. 2a and 2b). The generation of $^{1}O_2$ by the micellar aggregate in PBS was investigated by using 808 nm laser with 3 min irradiation, and the results were compared with **IR-Pyr**. Singlet oxygen sensor green (SOSG) was used to monitor the singlet oxygen generation ability of the micellar aggregate, which showed an enhancement in the fluorescence intensity upon reaction with $^{1}O_2$. 10 µM solution

View Article Online
DOI: 10.1039/C7SC03169F

of compounds was mixed with equimolar solution of SOSG in independent experiments. The change in fluorescence intensity of SOSG at 530 nm was monitored after exciting at 504 nm before and after irradiating with laser light (808 nm, 200 $mWcm^{-2}$) at different time intervals. The enhanced emission of SOSG gives direct indication of increased generation of singlet oxygen in the medium, which showed higher ability of **HA-IR-Pyr** over **IR-Pyr** (Fig. 3a). This can be possibly due to the different photophysical environment of the micellar aggregate with respect to the molecular state. The fluorescent life time of **HA-IR-Pyr** (10.55 µs) was longer than that of **IR-Pyr** (9.4 µs), can be correlated with enhanced ROS generation in the aggregate.

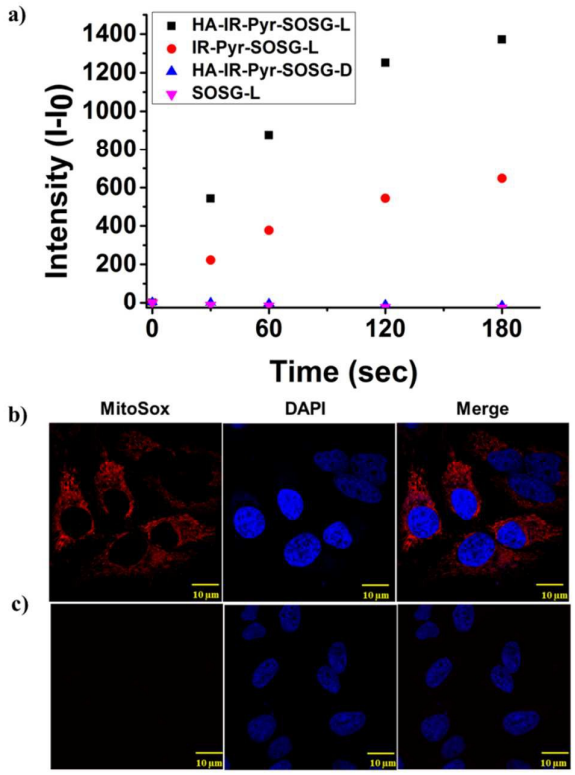

Fig. 3 Comparison of $^1O_2$ generation ability in a) PBS, b) HeLa cell lines after 3 min. irradiation c) HeLa cell lines without irradiation

Cancer-mitochondria-targeting using HA-IR-Pyr

As mitochondria are important regulators of cell death, PDT induced cytotoxicity within the mitochondria is found to be promising treatment modality. We investigated cellular uptake and mitochondrial accumulation of IR-Pyr in both cancerous (HeLa) and non-cancerous (HeK293T) cell lines, and compared with IR-780 (Fig. S17). The Pearson's co-localization coefficient for mitochondria localization was 0.61 and 0.73 for IR-780 and **IR-Pyr** respectively. However, both compounds accumulated in the non-cancerous cells as well, which is undesirable for an efficient therapeutic technique. In contrast, **HA-IR-Pyr** showed cancer selectivity and localized preferably in cancer mitochondria (Fig. 4). Confocal images after 4 h incubation with **HA-IR-Pyr** showed extensive accumulation in HeLa cell lines (Pearson's co-localization 0.77), while showed negligible accumulation in HeK293T cell lines. The selectivity of **HA-IR-Pyr** toward HeLa cell lines is attributed to the overexpression of CD44 in the cell lines (Fig S18). Further, the hyaluronidase enzyme could cleave the HA in the micellar aggregate, accelerating the release of **IR-Pyr** inside the cell.[10]

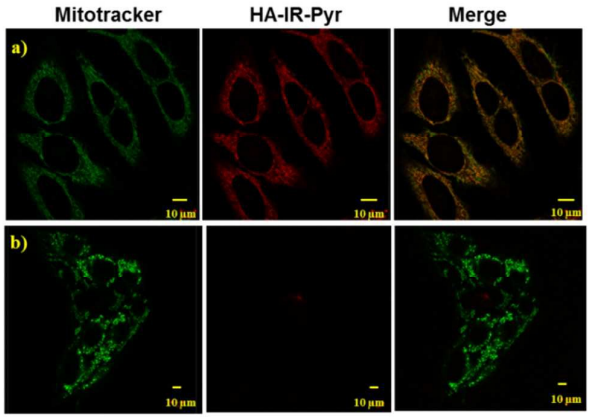

Fig. 4 Confocal images for analyzing mitochondria co-localization of **HA-IR-Pyr** in a) HeLa cell lines and b) HeK-293T cell lines.

Significance of HA and cellular uptake mechanism

The significance of HA coating for selective cellular uptake was further investigated with and without pretreatment of free HA. The confocal images showed that cellular accumulation in HeLa cell line was significantly less for free HA-pretreated samples than that were not pretreated (Fig. S19). However, there were no significant differences between free HA-pretreated and non-treated HeK293T cell lines, with the uptake being low in both cases (Fig. S20). This clearly implies that the HA- coated dye selectively accumulates in cancer cell lines attributed to the overexpression of HA receptors. Further, the dye did not accumulate in free HA pretreated HeLa cells attributable to competitive effect. We studied the cellular uptake mechanism in detail. Endocytosis is a common mechanism underlying the cellular uptake of nanoparticles that is implemented via various mediators such as clathrin, caveolae and macropinocytosis. The uptake mechanism of **HA-IR-Pyr** in HeLa cells was determined using confocal imaging with various endocytosis inhibitors such as sucrose for inhibiting clathrin mediated endocytosis, methyl-β-cyclodextrin (M-βCD) for caveolae and amiloride for macropinocytosis mediated cellular uptake. The confocal images showed that the uptake mechanism is controlled by macropinocytosis and clathrin mediated endocytosis (Fig. S21).

View Article Online
DOI: 10.1039/C7SC03169F

In vitro PDT experiments

The high mitochondrial accumulation and selectivity toward cancer cells were promising to conduct further experiments to investigate the PDT application of the micellar aggregate. Intracellular ROS generation during photoirradiation of **HA-IR-Pyr** was confirmed using confocal imaging. **HA-IR-Pyr** (2.5 µM) was incubated with HeLa cell lines for 2 h. ROS indicator (MitoSox Red) was added before irradiating with an 808 nm laser (200 $mWcm^{-2}$) for 3 min. The bright red fluorescent images from the confocal microscopy confirmed the generation of singlet oxygen inside the cell (Fig. 3b). A control experiment without photoirradiation did not produce any significant signal intensity indicating the photocontrolled generation of ROS (Fig. 3c). However, control experiment with IR-780 showed no remarkable difference between the laser irradiated and non-irradiated cells (Fig. S22), attributed to its inherent dark toxicity.

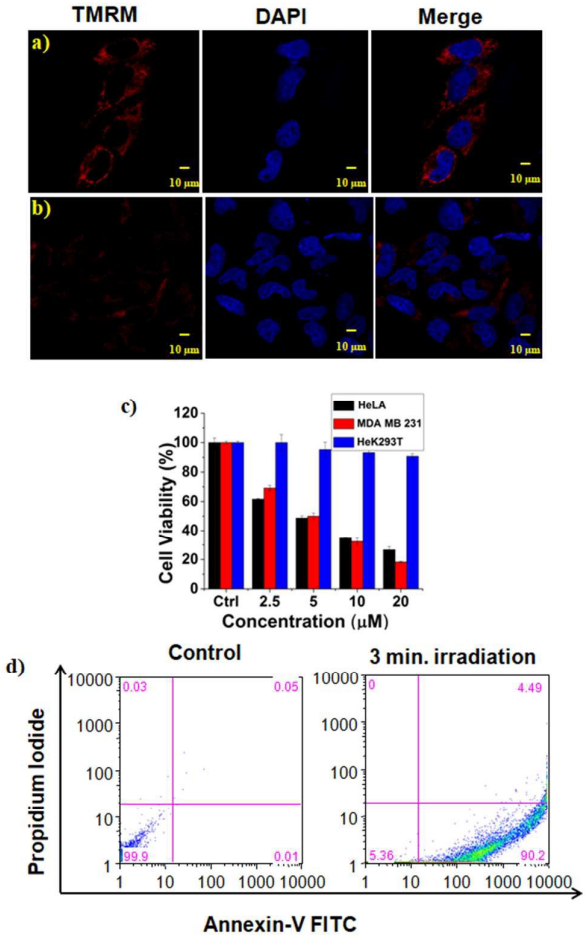

Fig. 5 Effect of PDT using **HA-IR-Pyr** after 3 min irradiation. a) mitochondrial membrane depolarization analysis using TMRM, c) dark toxicity of **HA-IR-Pyr**, and d) flow cytometry analysis comparing the extent of apoptosis before and after irradiation in HeLa cell lines with **HA-IR-Pyr**.

In addition, the mitochondrial damage during PDT was investigated by measuring differences in mitochondrial membrane potential during the photoirradiation and singlet oxygen generation. Analyses of mitochondrial membrane depolarization using TMRM showed visible difference in HeLa cell lines during PDT with **HA-IR-Pyr**, as reflected by the fluorescence turn off from TMRM (Fig. 5b). However, without irradiation the mitochondria were found to be intact (Fig. 5a). These results assure the PDT driven destruction of mitochondria.

Cell viability analyses after PDT with **HA-IR-Pyr** (808 nm laser, 3 min. irradiation, 200 $mWcm^{-2}$) were conducted in HeLa, MDA-MB-231 cell lines (cancerous models), and HeK293T cell lines (non-cancerous model) (Fig. 5c and Fig S 23). The alamar blue assay showed that **HA-IR-Pyr** induced cytotoxicity in a concentration dependent manner in the cancer lines (HeLa and MDA-MB-231) after photoirradiation, whereas it did not induce remarkable changes in the Hek293T cell lines due to lack of accumulation in the non-cancerous model. The IC50 was found to be 5-7 µM in both HeLa and MDA-MB-231 cell lines, whereas dark control experiments showed more than 85% viability, implying the efficient PDT effect of **HA-IR-Pyr**. In contrast, IR-780 showed significant dark toxicity in HeLa, MDA-MB-231 and HeK293T cell lines (Fig. S24). Further, the extent of apoptosis during PDT was determined by flow cytometry analysis using propidium iodide and annexin V. These data showed that 90% apoptosis population (Fig. 5e) after PDT with **HA-IR-Pyr**, whereas the dark control experiment showed no significant apoptotic cell population, inferring to an apoptosis mediated cell death during PDT.

In vivo imaging and PDT experiments

In vivo tumor imaging with **HA-IR-Pyr** was performed in SCC7 tumor xenograft model, which is important in PDT to localize the tumor and external time control on irradiation. The tumor imaging ability was compared with **IR-Pyr** and IR-780. Compounds were intravenously injected into tumor bearing mice (one mouse per group) and imaged at several time points using an optical imaging system by setting the excitation at 760 nm and emission at 830 nm. We found that **HA-IR-Pyr** preferentially accumulated in the tumor after 6 to 8 h, whereas the control molecules (**IR-Pyr** and IR-780) did not accumulate in tumor to show sufficient fluorescence signal (Fig. 6a, Fig. S25). The increased accumulation of **HA-IR-Pyr** was attributed to the overexpressed CD44 in the SCC7 tumor model, which is in agreement with the in vitro studies using CD44 positive cells.

The PDT efficacy of **HA-IR-Pyr** was investigated in vivo after injecting the micellar aggregate intravenously into SCC7 tumor-bearing mice. An NIR laser (808 nm) was selected and low power irradiation (200 $mWcm^{-2}$) was used as an excitation source to activate **HA-IR-Pyr** for in vivo PDT. Four groups of tumor-bearing mice were subjected to different treatments PBS + L (with light irradiation), PBS (without light irradiation), HA-IR-Pyr + L (with light irradiation) and HA-IR-

View Article Online
DOI: 10.1039/C7SC03169F

Pyr (without light irradiation) with four mice per group. **HA-IR-Pyr** accumulation at the tumor sites reached its maximum at 8h, at which time the selected groups were irradiated with NIR laser (200 $mWcm^{-2}$) for 3 min. Phototoxicity of the micellar aggregate to the tumor was assessed by monitoring the relative tumor volumes and body weight changes. As shown in Fig. 6b, no significant changes in body weight were noted in HA-IR-Pyr and control groups with and without laser irradiation, indicating minimum side effects during PDT with the micellar aggregate.

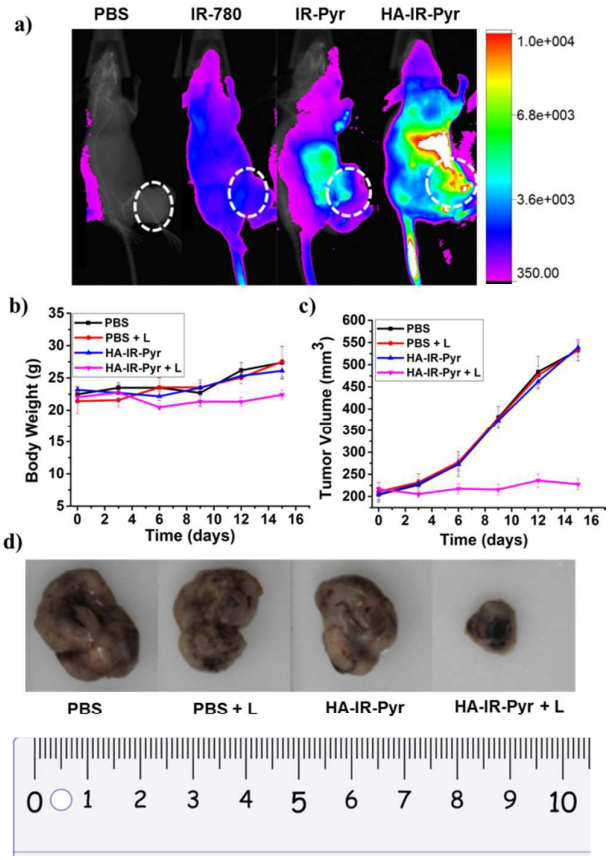

Fig.6 a) Accumulation of **HA-IR-Pyr** in SSC7 tumor model after 8h in comparison with other control molecules, b) changes in body weight with time during PDT, c) change in the tumor volumes with time during PDT and d) comparison of the tumor size after 16 days.

Tumor volume measurements showed clear differences in tumor growth between the HA-IR-Pyr + L group and the control groups (Fig. 6c, 6d, S26, and S27). No tumor reduction was observed in the control groups (PBS + L and PBS). Similarly, HA-IR-Pyr (dark control) showed negligible toxicity in the dark. In marked contrast, significant tumor growth inhibition was observed in HA-IR-Pyr + L groups and tumor tissue showed obvious cell death. The treatment efficiency, in terms of tumor cell death was also evaluated by hematoxylin and eosin (H & E) staining of tumor tissue sections. After 16 d, both the PDT treated and the untreated mice were sacrificed for H & E staining. Noticeable signs of difference was observed between the control groups [PBS + L, PBS and HA-IR-Pyr), and the HA-IR-Pyr + L group, as shown in Fig. 7. These results assured high PDT efficacy of **HA-IR-Pyr** micellar aggregates in the in vivo model with minimum dark toxicity.

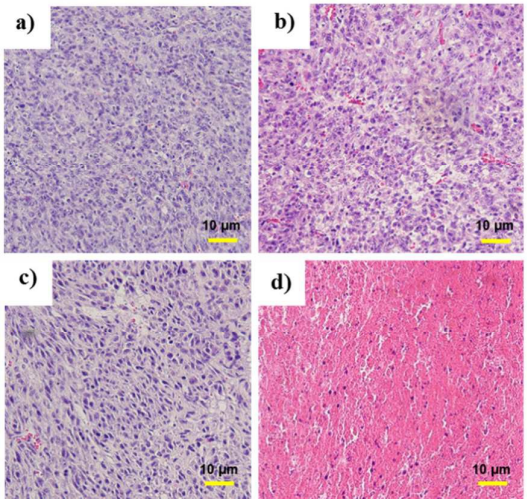

Fig. 7 H and E stained section of tumor after treating with, a) PBS b) PBS + L, c) HA-IR-Pyr and d) HA-IR-Pyr + L

Conclusions

In conclusion, we developed **IR-Pyr**, a mitochondria targeting, water soluble indocyanine dye for PDT application. Incorporation of pyridinium ion into the indocyanine skeleton increased the water solubility that prevents aggregation and provides increased dark and photostability than that of IR-780. The overall positive charge is increased from one to three that enhanced the mitochondria targeting ability in comparison with IR-780. Further, the construction of an HA coated micellar aggregate; **HA-IR-Pyr** provided cancer targeting ability that lead to a cancer-mitochondria-targeted PDT. The singlet oxygen generation efficiency of the micellar aggregate was better than that of the free dye **IR-Pyr**, reflecting results of the in vitro and in vivo PDT experiments. These results discussed here showcase the importance of mitochondria targeted PDT, and would aid in the development of molecular systems with higher therapeutic efficacy.

Acknowledgements

This work was supported by the Korea Foundation for the Advancement of Science & Creativity (KOFAC), and funded by the National Research Foundation of Korea (2017R1A2B4003617, 2016R1D1A1B03933931 and 2016R1A5A1009405).

View Article Online
DOI: 10.1039/C7SC03169F

Notes and references

Authors declare no competing financial interest.

1 (a) A. P. Castano, P. Mroz and M. R. Hamblin, *Nat. Rev.* 2006, **6**, 535; (b) S. Kim, T. Ohulchanskyy, H. Pudavar, R. Pandey and P. Prasad, *J. Am. Chem. Soc.* 2007, **129**, 2669; (c) M. Ethirajan, Y. Chen, P. Joshi and R. K. Pandey, *Chem. Soc. Rev.* 2011, **40**, 340; (d) Y. Wang, G. Wei, X. Zhang, F. Xu, X. Xiong and S. Zhou, *Adv. Mater.* 2017, **29**, 1605357; (e) S.-Y. Li, W.-X. Qiu, H. Cheng, F. Gao, F.-Y. Cao and X.-Z. Zhang, *Adv. Funct. Mater*. 2017, **27**, 1604916; (f) A. P. Thomas, P. S. Saneesh Babu, S. Asha Nair, S. Ramakrishnan, D. Ramaiah, T. K. Chandrashekar, A. Srinivasan and M. Radhakrishna Pillai, *J. Med. Chem.* 2012, **55**, 511; (g) J. Ge, M. Lan, B. Zhou, W. Liu, L. Guo, H. Wang, Q. Jia, G. Niu, X. Huang, H. Zhou , X. Meng, P. Wang, C.-S. Lee, W. Zhang and X. Han, *Nat. Commun*. 2014, **5**, 1; (h) E. Ju, K. Dong, Z. Chen, Z. Liu, C. Liu, Y. Huang, Z. Wang, F. Pu, J. Ren and X. Qu, *Angew. Chem. Int. Ed.* 2016, **55**, 11467.

2 (a) J. P. Celli, B. Q. Spring, I. Rizvi, C. L. Evans, K. S. Samkoe, S. Verma, B. W. Pogue and T. Hasan, *Chem. Rev.* 2010, **110**, 2795; (b) X. Li, S. Kolemen, J. Yoon and E. U. Akkaya, *Adv. Funct. Mater*. 2017, **27**, 1604053; (c) K. Lang, J. Mosinger and D. M. Wagnerova, *Coord. Chem. Rev*. 2004, **248**, 321.

3 (a) J. F. Lovell, T. W. B. Liu, J. Chen and G. Zheng, *Chem. Rev.* 2010, **110**, 2839.

4 (a) H. Chen, J. Tian, W. He and Z. Guo, *J. Am. Chem. Soc*. 2015, **137**, 1539; (b) C. Hopper, *Lancet. Oncol.* 2000, **1**, 212; (c) S. B. Brown, E. A. Brown and I. Walker, *Lancet. Oncol.* 2004, **5**, 497.

5 H. S. Jung, J. Han, H. Shi, S. Koo, H. Singh, H. –J. Kim, J. L. Sessler, J. Y. Lee, J. –H. Kim and J. S. Kim, *J. Am. Chem. Soc.* 2017, **139**, 7595.

6 (a) S. E. Weinberg and N. S Chandel, *Nat. Chem. Bio*. 2015, **11**, 9; (b) S. Gupta, G. E. N. Kass, E. Szegezdi and B. Joseph, *J. Cell. Mol. Med*. 2009, **13**, 1004; (c) C. Lee, H.-K. Park, H. Jeong, J. Lim, A.-J. Lee, K. Y. Cheon, C.-S. Kim, A. P. Thomas, B. Bae, N. D. Kim, S. H. Kim, P.-G. Suh, J.-H. Ryu and B. H. Kang, *J. Am. Chem. Soc*. 2015, **137**, 4358; (d) H. S. Jung, J. –H. Lee, K. Kim, S. Koo, P. Verwilst, J. L. Sessler, C. Kang and J. S. Kim, *J. Am. Chem. Soc.* 2017, DOI: 10.1021/jacs.7b04263.

7 (a) S. Chakrabortty, B. K. Agrawalla, A. Stumper, N. M Vegi, S. Fischer, C. Reichardt, M. Kögler, B. Dietzek, M. F. Buske, C. Buske, S. Rau and T. Weil, *J. Am. Chem. Soc*. 2017, **139**, 2512; (b) L. Rui, Y. Xue, Y. Wang, Y. Gao and W. Zhang, *Chem. Commun*. 2017, **53**, 3126; (c) R. Guo, H. Peng, Y. Tian, S. Shen and W. Yang, *Small* 2016, **12**, 4541; (d) K. Han, Q. Lei, S.-B. Wang, J.-J. Hu, W.-X. Qiu, J.-Y. Zhu, W.-N. Yin, X. Luo and X.-Z. Zhang, *Adv. Funct. Mater*. 2015, **25**, 2961; (e) W. Lv, Z. Zhang, K. Y. Zhang, H. Yang, S. Liu, A. Xu, S. Guo, Q. Zhao and W. Huang, *Angew. Chem. Int. Ed.* 2016, **55**, 9947.

8 (a) S. Luo, X. Tan, Q. Qi, Q. Guo, X. Ran, L. Zhang, E. Zhang, Y. Liang, L. Weng, H. Zheng, T. Cheng, Y. Su and C. Shi, *Biomaterials* 2013, **34**, 2244; (b) E. Zhang, S. Luo, X. Tan and C. Shi, *Biomaterials* 2014, **35**, 771; (c) X.Tan, S. Luo, D. Wang, Y. Su, T. Cheng and C. Shi, *Biomaterials* 2012, **33**, 2230.

9 (a) V. Saxena, M. Sadoqi and J. Shao, *J. Pharm. Sci.* 2003, *92*, 2090; (b) H. V. Berlepsch and C. Böttcher, *J. Phys. Chem. B* 2015, **119**, 11900.

10 (a) D. K. Chatterjee, L. S. Fong and Y. Zhang, *Adv. Drug Deliv. Rev*. 2008, **60**, 1627; (b) P. Kalluru, R. Vankayala, C.-S. Chiang and K. C. Hwang, *Angew. Chem. Int. Ed.* 2013, **52**, 12332; (c) J. A. Barreto, W. O'Malley, M. Kubeil, B. Graham, H. Stephan and L. Spiccia, *Adv. Mater*. 2011, **23**, 18; (d) C. Yue, P. Liu, M. Zheng, P. Zhao, Y. Wang , Y. Ma and L. Cai, *Biomaterials* 2013, **34**, 6853; (e) K. Wang, Y. Zhang, J. Wang, A. Yuan, M. Sun and J. Wu, *Sci. Rep*. 2016, **6**, 27421; (f) Y. Chen, Z. Li, H. Wang, Y. Wang, H. Han, Q. Jin and J. Ji, *ACS Appl. Mater. Interfaces* 2016, **8**, 6852. (g) A.Yuan, X. Qiu, X. Tang, W. Liu, J. Wu and Y. Hu, *Biomaterials* 2015, **51**, 184.

11 (a) G. Wang, F. Zhang, R. Tian, L. Zhang, G. Fu, L. Yang and L. Zhu, ACS Appl. Mater. Interfaces 2016, 8, 5608−5617; (b) H. Gong, Y. Chao, J. Xiang, X. Han, G. Song, L. Feng, J. Liu, G. Yang, Q. Chen and Z. Liu, *Nano Lett.* 2016,**16**, 2512.